Dynamic periplasmic chaperone reservoir facilitates biogenesis of outer membrane proteins

Shawn M. Costello[a], Ashlee M. Plummer[a], Patrick J. Fleming[a], and Karen G. Fleming[a,1]

[a]T. C. Jenkins Department of Biophysics, Johns Hopkins University, Baltimore, MD 21218

Edited by William F. DeGrado, School of Pharmacy, University of California, San Francisco, CA, and approved June 29, 2016 (received for review January 19, 2016)

Outer membrane protein (OMP) biogenesis is critical to bacterial physiology because the cellular envelope is vital to bacterial pathogenesis and antibiotic resistance. The process of OMP biogenesis has been studied in vivo, and each of its components has been studied in isolation in vitro. This work integrates parameters and observations from both in vivo and in vitro experiments into a holistic computational model termed "Outer Membrane Protein Biogenesis Model" (OMPBioM). We use OMPBioM to assess OMP biogenesis mathematically in a global manner. Using deterministic and stochastic methods, we are able to simulate OMP biogenesis under varying genetic conditions, each of which successfully replicates experimental observations. We observe that OMPs have a prolonged lifetime in the periplasm where an unfolded OMP makes, on average, hundreds of short-lived interactions with chaperones before folding into its native state. We find that some periplasmic chaperones function primarily as quality-control factors; this function complements the folding catalysis function of other chaperones. Additionally, the effective rate for the β-barrel assembly machinery complex necessary for physiological folding was found to be higher than has currently been observed in vitro. Overall, we find a finely tuned balance between thermodynamic and kinetic parameters maximizes OMP folding flux and minimizes aggregation and unnecessary degradation. In sum, OMPBioM provides a global view of OMP biogenesis that yields unique insights into this essential pathway.

β-barrel | OMP biogenesis | BAM | kinetic model | membrane protein folding

The cellular envelope of Gram-negative bacteria is comprised of two membranes separated by an aqueous compartment termed the "periplasm." The outer membrane of the cellular envelope contains integral β-barrel membrane proteins referred to as "outer membrane proteins" (OMPs) (1, 2). The outer membrane and OMPs provide the first barrier between bacteria and the environment and are essential to many important cellular processes including metabolic transport, bacterial virulence, and antibiotic resistance (3–5). Understanding the pathway by which OMPs traverse the periplasm and attain their native functional state is essential to an ability to manipulate this element of the bacterial cell.

The OMP biogenesis process is distinct from the folding of cytosolic proteins because it involves a unique collection of obstacles. First, OMPs do not adopt their folded conformations while in an aqueous environment (6). Rather, unfolded OMPs (uOMPs) must be transported across the periplasm to reach their native membrane. Because of their marginal solubility in water, this process must be tightly controlled to avoid aggregation. Second, structures of folded OMPs (fOMPs) show that these proteins contain water-solvated residues in loops on the outer surfaces of bacteria. The desolvation and transport of these polar and ionizable side chains across the outer membrane represent significant kinetic barriers to OMP folding (7). Third, Gram-negative bacteria maintain a high density of fOMP in the expanding outer membrane (8) that requires a considerable flux of uOMP transport across the periplasm followed by folding to replace OMP lost to dilution during growth (9). Finally, all periplasmic chaperones, proteases, and folding machinery must operate without the free energy provided by ATP hydrolysis, unlike cytosolic proteins with similar roles (10).

Because of the important cellular functions and the unique biogenesis pathway of OMPs, considerable effort has been applied to understanding the process of OMP folding and assembly. Many in vitro and in vivo studies have investigated various components involved in this pathway (11–22). However, in vitro experiments typically characterize individual components in isolation, and in vivo studies are often incapable of deciphering how specific components are responsible for observed phenomena. Computational techniques can overcome these limitations by combining orthogonal sets of information and allowing unique system-wide studies of multiprotein networks. This holistic approach is especially important when multiple competing reactions occur, as in the transit of uOMPs through the periplasm of Gram-negative bacteria. In this cellular compartment, at least four distinct complexes can form between uOMPs and chaperones [e.g., uOMP binding to Skp (17-kDA protein), SurA (survival factor A), FkpA (FKPB-type peptidyl-prolyl *cis-trans* isomerase FkpA), or DegP (periplasmic serine endoprotease DegP)], and the emergent properties of periplasmic proteostasis cannot be evaluated without a consideration of this linkage. To date, no computational study has investigated OMP biogenesis in this comprehensive manner, but this biological system is ideal for this type of analysis because many of the relevant protein species have been well studied in isolation (for review, see ref. 2).

Toward this end, we created a single comprehensive mathematical framework, Outer Membrane Protein Biogenesis Model (OMPBioM), which incorporates known kinetic and thermodynamic parameters for many of the reactions related to uOMP transport across the periplasm. We used both deterministic and

Significance

The study of bacterial outer membrane proteins (OMPs) is critical to understanding cellular communication, metabolic transport across membranes, and pathogenesis. We used a holistic computational approach to examine how the OMP biogenesis machinery maintains cellular proteostasis under biologically relevant conditions. This treatment overcomes common limitations of both in vitro and in vivo experiments because we can simultaneously investigate unfolded OMP (uOMP) transport and folding trajectories at a microscopic level and phenotypes at a macroscopic level. This analysis provides global insight into the dynamic process of periplasmic uOMP transport and highlights the unique contributions of individual chaperones in the maintenance of outer membrane and periplasmic proteostasis.

Author contributions: S.M.C., A.M.P., P.J.F., and K.G.F. designed research; S.M.C. performed research; S.M.C. analyzed data; and S.M.C., A.M.P., P.J.F., and K.G.F. wrote the paper.

The authors declare no conflict of interest.

This article is a PNAS Direct Submission.

[1]To whom correspondence should be addressed. Email: karen.fleming@jhu.edu.

This article contains supporting information online at www.pnas.org/lookup/suppl/doi:10.1073/pnas.1601002113/-/DCSupplemental.

stochastic methods to calculate the time-dependent trajectories of uOMPs in the periplasm, to simulate and reproduce several single- and double-null strain phenotypes as well as the σ^E stress response, to gain insight into periplasmic dynamics between uOMPs and chaperones, and to predict limits for the effective rate of β-barrel assembly machinery (BAM)-assisted OMP folding. We discovered that OMP biogenesis involves timescales that are much longer than those of chaperone–uOMP complexes. Hundreds of chaperone–uOMP binding and unbinding events take place before uOMP folding, suggesting that chaperone–uOMP binding reactions are near equilibrium in the periplasm. Moreover, we find that periplasmic chaperones have distinct roles that complement each other, resulting in preferential flux to folding through a SurA–BAM catalyzed folding pathway. Finally, intricate mechanisms for OMP transport and folding that involve higher-order complexes that span the width of the periplasm or that contain parallel chaperone folding pathways with comparable flux are not required to reproduce current experimental observations.

Results

OmpBioM Reproduces Experimentally Observed fOMP Levels and uOMP Periplasmic Lifetimes. Fig. 1 shows the set of linked reactions involved in OMP biogenesis that we incorporated for this mechanistic investigation. OMPBioM deterministically simulates the biogenesis of a representative uOMP using parameters derived from direct observations of *Escherichia coli* or from in vitro experiments using *E. coli* proteins. *SI Appendix*, Tables S1 and S2 list the relevant rate constants and kinetic equations. We used cellular concentrations of known species (23) to reproduce key experimental observables: genetic phenotypes, OMP copy number per cell, and uOMP periplasmic lifetime.

Under WT conditions, the area density of fOMP in the outer membrane has been reported to be high, with a copy number per cell between 8,000 and 80,000 (23, 24). Others have shown that the periplasmic lifetime of a representative uOMP (i.e., LamB) is approximately 2 min (25). We used these fOMP levels and the periplasmic uOMP lifetime to assess the validity of our treatment of this system. Fig. 2 shows the WT phenotype in which we obtain a fOMP copy number equal to 28,000, which agrees well with the known experimental values. Similarly, quantitation of the periplasmic uOMP lifetime yields an average of 1 min in WT cells (*SI Appendix*, Fig. S3*A* and Table S4), also in excellent agreement with the magnitude observed in vivo.

Single-Chaperone–Null Mutant Phenotypes Reveal the Importance of SurA Activity and σ^E Response. We used the reaction scheme outlined in Fig. 1 to simulate genetic mutants lacking specific chaperones. Four distinct single-chaperone–null strain simulations (Δ*degP*, Δ*skp*, Δ*fkpA*, or Δ*surA*) were independently performed and compared with the WT simulations and with known biological phenotypes (11–13). Fig. 2 shows that the individual Δ*degP*, Δ*skp*, and Δ*fkpA* simulations display fOMP and free and aggregated uOMP concentration profiles similar to WT profiles under normal growth conditions. These results are consistent with the modest phenotypic effects observed in genetic studies of the null strains for each corresponding chaperone (11).

In contrast, SurA is the only single periplasmic chaperone that is known to cause a significant change in fOMP density when depleted (11, 13). Our simulations capture this genetic finding (Fig. 2). The importance of SurA in OMP biogenesis arises from its dual functions, both of which are incorporated in OMPBioM: (*i*) SurA can bind to uOMP, thereby preventing aggregation, and (*ii*) SurA can facilitate the folding of uOMP (13–17, 22). Because SurA plays a prominent role in OMP folding, the loss of SurA in vivo results in the induction of the σ^E stress response (11, 13), a regulatory mechanism caused by the accumulation of unfolded protein in the periplasm. For Δ*surA*, activation of this envelope stress response results in an increase in chaperone expression and a reduction in uOMP expression; these experimental observations are incorporated into our Δ*surA* simulation (*SI Appendix*, Table S3) (26, 27).

To investigate further the role of the σ^E response in managing cellular fitness, we performed *surA*-null simulations in both the absence (Δ*surA**) and presence (Δ*surA*) of a computational treatment of σ^E (*SI Appendix*, Fig. S4). The hypothetical Δ*surA** mutant has not been observed in vivo. Therefore, a computational comparison between the WT and Δ*surA** phenotypes provides an opportunity to observe the molecular damage that may stimulate an *E. coli* envelope stress response. *SI Appendix*,

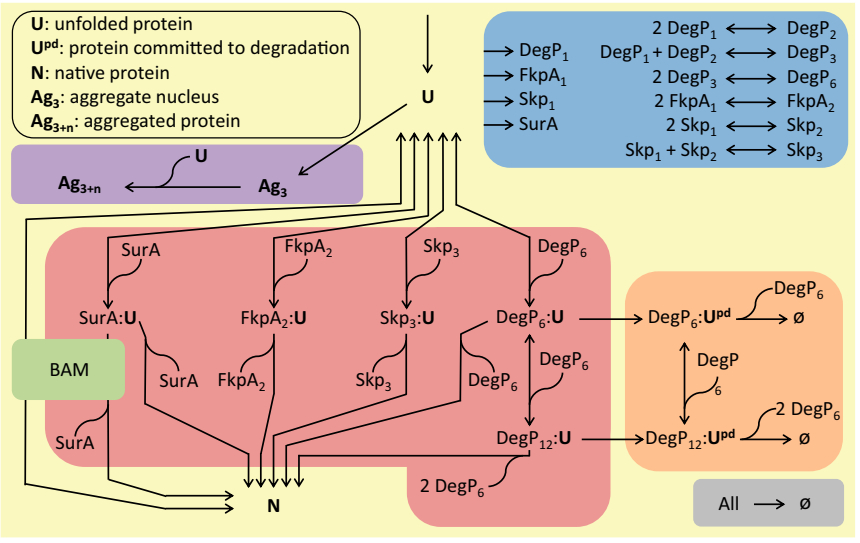

Fig. 1. Diagram of mechanistic treatment used in OMPBioM. The downward vertical arrow at the top of the figure indicates uOMP synthesis and translocation. Nascent uOMP (U) can interact with itself through the aggregation pathway (purple), bind to chaperone (red) before folding into its native state (N), or be degraded (orange). Chaperones enter the system as monomers before undergoing oligomerization into a binding-competent oligomerization state indicated by subscript (blue). All species are subject to a rate of dilution (gray). Chaperones are regenerated upon uOMP folding or unbinding. Folding pathways that are assumed to be accelerated by BAM are shown (green). For more information of this mechanistic treatment see *SI Appendix*.

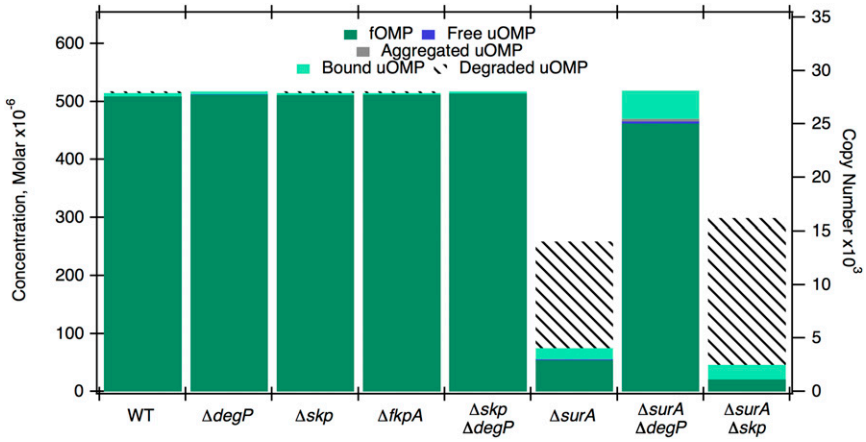

Fig. 2. Trends observed in the simulated and experimentally observed phenotypes agree. The steady-state concentrations of each OMP species in the simulations for the WT and indicated chaperone single- and double-null mutants are shown. Species include fOMP (dark green), free monomeric uOMP (blue), aggregated uOMP (gray), bound uOMP (light green), and degraded uOMP (hatched segments). Bound uOMP is the sum of uOMP bound to all chaperones, including SurA, Skp, FkpA, and DegP. The *x* axis indicates simulated phenotypes. Simulations indicate that minimal populations of free and aggregated uOMP are present under WT and mild phenotype conditions. Simulated σ^E responses are included for Δ*surA*, Δ*surA*Δ*degP*, and Δ*surA*Δ*skp*. Data are provided in tabular form in *SI Appendix*, Table S6.

Figs. S4 and S5 show that the virtual Δ*surA** results in a reduction in fOMP and a 290-fold increase in the sum of free and aggregated uOMP compared with WT, as is consistent with suggestions that the accumulation of periplasmic uOMPs stimulates the induction of the σ^E response (28).

To mimic the consequences of the stress response in the biologically relevant Δ*surA* phenotype, we parameterized OMP synthesis rates and chaperone levels to return fOMP amounts equivalent to those observed in vivo. *SI Appendix*, Fig. S4 shows this reduction in fOMP in Δ*surA* compared with WT; this result agrees with experiments (13, 15). In addition, *SI Appendix*, Fig. S5 shows that the incorporation of a stress response relieves the nearly 300-fold increase in the sum of free and aggregated uOMP populations predicted by Δ*surA**. Moreover, although these populations are lower with the stress response, they are not completely eradicated and are still ∼10-fold higher than WT levels. This finding, too, is consistent with the biologically observed Δ*surA* phenotype in which uOMP accumulates in the periplasm although the conditions are still conducive to growth (11, 13). In addition, the average periplasmic lifetime of an OMP in vivo is 10-fold longer in Δ*surA* than in WT (25), as is consistent with our observation that the average periplasmic lifetime in simulated Δ*surA* is 15-fold greater than that predicted for WT (*SI Appendix*, Table S4). In sum, the agreement between the trends observed in vivo and in simulations for the implementation of Δ*surA* incorporating a σ^E response further validates the mechanism and parameters used for SurA function and our simulated σ^E response.

Simulations of Double-Chaperone–Null Strains Suggest Distinct Roles for Skp and DegP. Double-null strains obtained by either gene deletion or depletion of periplasmic chaperones have documented phenotypes that can be more severe than those of single-null mutants (15, 29). In vivo, the absence of either DegP or Skp concurrent with the absence of SurA (e.g., Δ*surA*Δ*degP* or Δ*surA*Δ*skp*) results in a phenotype more severe than the phenotypes for Δ*surA*, Δ*degP*, Δ*skp*, or Δ*skp*Δ*degP*. This result implies that the activities of Skp and DegP are more important in a Δ*surA* genetic background than in a WT cell and has been interpreted as evidence of parallel folding pathways in OMP biogenesis (15, 29). To investigate the roles of these chaperones, we simulated and compared the phenotypes of the double-null mutants Δ*skp*Δ*degP*, Δ*surA*Δ*degP*, and Δ*surA*Δ*skp* with a simulated σ^E stress response and appropriate doubling times (Fig. 2 and *SI Appendix*, Table S3). Overall we found phenotypes consistent with in vivo observations. Fig. 2 shows that, similar to each of the single-null mutants, Δ*skp*Δ*degP* is viable with minimal phenotypic consequences (11, 12), whereas Δ*surA*Δ*skp* and Δ*surA*Δ*degP* mutants (both incorporating σ^E) show either an increase in free and aggregated uOMP or a decrease in the concentration of fOMP relative to the single Δ*surA* mutant (Fig. 2 and *SI Appendix*, Fig. S5); these findings also are consistent with experimental results (13, 15).

In addition, we observe a large fraction of degraded protein in the Δ*surA*Δ*skp* simulation (∼85%) (Fig. 2, hatched bars and *SI Appendix*, Fig. S6). This degradation is attributed not only to the presence of the protease DegP (30–32) but also to the large population of free uOMP available for proteolysis. In contrast, free uOMP cannot be degraded in the Δ*surA*Δ*degP* simulation because DegP is absent, and OMP can only fold independently of SurA, aggregate, or dilute away. As a consequence, Δ*surA*Δ*degP* displays an increase in the fOMP population compared with either Δ*surA* or Δ*surA*Δ*skp*, as is consistent with in vivo findings (15).

DegP Functions Primarily as a Protease and Is Under Kinetic Control. Although DegP has been suggested to function both as a chaperone and as a protease (30, 32, 33), our results from double-null simulations suggest that the chaperone activity of DegP is not a significant contributor to OMP biogenesis. This conclusion is further supported by results from stochastic simulations that allow enumeration of chaperone–uOMP binding events. DegP is involved in <0.02% of the binding events under WT conditions and <0.4% of uOMP binding events under Δ*surA* conditions (*SI Appendix*, Table S4). These low percentages suggest that the chaperone activity of DegP may be negligible under all tested conditions.

In what may seem like a contradiction, a significant fraction of uOMP is degraded under stressful conditions, with 71% and 85% of secreted uOMP degraded in the Δ*surA* and Δ*surA*Δ*skp* simulations, respectively (*SI Appendix*, Fig. S6). This phenomenon is a testament to the kinetic partitioning present in this system, with the relatively slow binding of DegP to uOMP substrate and the even slower dissociation of DegP being equally important (*SI Appendix*, Table S1). The low population of uOMP, the presence of other chaperones, and slow binding together prevent DegP from binding to and degrading uOMP under WT conditions, as evidenced by the low fraction bound and the infrequent binding

events observed (*SI Appendix*, Fig. S7 and Table S4). However, under stress conditions the high population of free periplasmic uOMP (a 10-fold increase in Δ*surA*) (*SI Appendix*, Fig. S5) and the prolonged periplasmic OMP lifetime (*SI Appendix*, Table S4) allow a small but significant number of DegP binding events to occur. A high fraction of these binding events result in the degradation of the uOMP substrate, because the timescales for DegP dissociation and degradation are similar. Therefore, the binding, dissociation, and degradation rates for DegP measured in vitro are capable of preventing the unnecessary degradation of uOMP under WT conditions while also allowing the degradation of substrate and alleviation of uOMP accumulation under stress conditions.

Skp-uOMP Complexes Are Highly Populated and Display Dynamic Behavior. Skp is thought to act as a "holdase" by binding to and preventing the aggregation of uOMP in vitro (34–36). The binding of Skp to uOMP is thermodynamically favorable and kinetically fast (*SI Appendix*, Table S1). The favorable binding results in a large population of Skp–uOMP complex at steady state (*SI Appendix*, Fig. S7). However, the association rate of Skp to uOMP is nearly diffusion limited, and the dissociation rate is on the millisecond timescale (*SI Appendix*, Table S1). This dissociation timescale is several orders of magnitude shorter than the average periplasmic OMP lifetime under WT conditions, resulting in a large number of association and dissociation events for each OMP client (*SI Appendix*, Table S4). Therefore, to the extent that the term "holdase" implies a long-lived Skp–uOMP complex, its use is misleading. In contrast, the Skp–uOMP interactions are fleeting but populated to a significant extent. This dynamic nature of Skp binding should be considered when discussing the holdase activity. This specific binding kinetic behavior may play a unique role in controlling uOMP conformational populations. The unfolded client may explore a large configurational space, with certain conformations likely favoring either the folding or self-association reactions. We speculate that the fast binding to and dissociation from Skp may help promote folding-competent or aggregation-incompetent conformations.

The Folding Rate Enhancement Provided by SurA Is Necessary but Modest. SurA is the only soluble chaperone implicated in the in vivo folding of uOMP; therefore we investigated this reported "foldase" activity (37). OMPBioM treats the folding of a uOMP through the SurA–BAM pathway as faster than the BAM-only pathway. This change in folding rate is expressed using the term "rate enhancement," and this parameter is defined as the OMP folding rate through the SurA–BAM pathway divided by the OMP folding rate through BAM alone. To investigate the necessary magnitude of the rate enhancement provided by SurA, we concurrently varied this parameter with the BAM folding rate (k_{fold}). Fig. 3 shows this space (in cyan) bounded by the known range of OMP periplasmic lifetimes (in green) and further constrained by the summed concentration of free and aggregated uOMP (in red) and the previously reported phenotype range for Δ*surA* (in gray). The value of the rate enhancement must be between 3 and 100 to satisfy these constraints, with a WT value of 10. Interestingly, for this physiological range of folding rates and rate enhancements, the majority (between 80 and >99%) of uOMP folds through the SurA–BAM pathway, providing further evidence that SurA plays a key role in OMP biogenesis (*SI Appendix*, Fig. S8).

It is worth noting that a 10-fold rate enhancement is modest relative to common folding catalyst rate enhancements (38). This observation may provide insight into the foldase mechanism of SurA. We speculate that the previously observed binding of SurA to uOMP and the interaction of SurA and the BAM complex (14, 15, 17, 36) simply increase local concentrations, which then could be sufficient to provide the modest rate enhancement

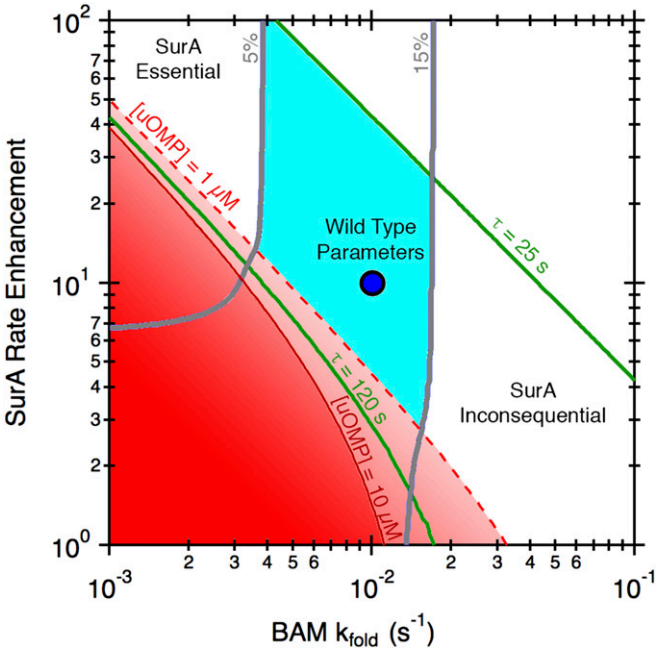

Fig. 3. A folding rate enhancement provided by SurA is required to recapitulate phenotypes. The rate enhancement provided by SurA is defined as the folding rate constant for SurA–BAM divided by the folding rate constant for BAM-only. Shown are contour lines for OMP periplasmic lifetime (green) and the summed concentration of free and aggregated uOMP (red). The concentration of fOMP in the Δ*surA* simulation and WT simulation are related; the Δ*surA* simulation is expected to return a concentration of fOMP ~10% of that in the WT simulation (13). The limits defining where the fOMP concentration in the Δ*surA* simulation is 5% or 15% of the WT simulation are shown as gray contour lines. If this value is less than 5%, SurA is more essential than expected; if the value is greater than 15%, SurA is more inconsequential than expected. The cyan area indicates the parameter space that results in lifetimes, free and aggregated uOMP concentrations, and fOMP concentrations that agree with experimental observations; a mild rate enhancement of 3–100 fold is required to recapitulate experimental observations.

needed to reproduce phenotypes. For this reason, we propose that the experimentally observed folding catalytic ability of SurA is not necessarily indicative of an intricate folding catalytic mechanism. The details of SurA-BAM–mediated OMP folding merit further biophysical investigation.

The Estimated Effective Rate of uOMP Folding by BAM is Faster than in Vitro Observations. The mechanistic details for how the BAM complex catalyzes uOMP folding are not well understood (20, 39–44). Even lacking this information, we can use OMPBioM to estimate the effective rate necessary for BAM-assisted OMP folding. This parameter must be large enough to prevent an accumulation of periplasmic uOMP but maintain a sufficient amount of fOMP under physiological uOMP synthesis and cellular replication rates. Under WT conditions, the BAM concentration is not rate limiting, as evidenced by the absence of a phenotypic effect when BamA levels are reduced 10-fold (45); therefore we do not explicitly consider BAM concentration effects. Fig. 4 shows multiple simulation outputs as a function of both the uOMP synthesis rate (k_{in}) and the BAM-mediated OMP folding rate (k_{fold}). Contour lines indicate physiological upper and lower bounds for the OMP periplasmic lifetime (green), fOMP copy number per cell (blue), and an upper bound of free and aggregated uOMP (red). Given these limitations, the effective OMP folding rate through the BAM pathway under WT conditions should range from $0.3–6 \times 10^{-2} \cdot s^{-1}$.

This value is consistent with the copy numbers for BamA and total OMP and the replication time for *E. coli*. For a cell

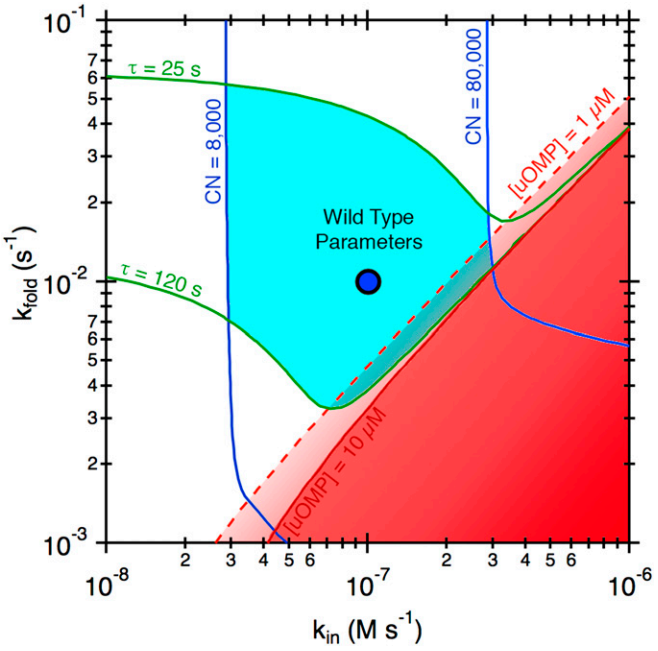

Fig. 4. OMPBioM allows the assessment of in vivo BAM folding rates. Shown are the contour lines for OMP periplasmic lifetimes (green) and copy number per cell (CN) (blue) as a function of covariation of the periplasmic input rate (k_{in}) and the effective BAM folding rate (k_{fold}). The parameter space allowed by the known values for OMP lifetimes and CN is shown in cyan. The dashed red line indicates the boundary where the concentration of free and aggregated uOMP in the periplasm equals 1 μM; this is a viable parameter space. The solid red line is the boundary at which uOMP + Aggregate = 10 μM; this concentration would be expected to induce the envelope stress response. The increasing red shading in the bottom right corner indicates the increasing accumulation of uOMP in the periplasm; these levels would be expected to lead to cell death.

containing 200 BamA molecules (23) and ∼28,000 fOMPs, the calculated turnover number for BamA would be 140 per cell generation. Assuming a generation time of 1 h, the expected rate would be $3.9 \times 10^{-2} \cdot s^{-1}$. This calculated first-order rate constant is in excellent agreement with the predicted range shown in Fig. 4.

It is noteworthy that this effective rate constant is currently not attainable in vitro. The predicted lower limit (i.e., $0.3 \times 10^{-2} \cdot s^{-1}$) is an order of magnitude faster than the rate observed for BAM protein A (BamA)-mediated OMP folding in nonnative lipid conditions (20) and the rate observed for SurA-BAM–assisted in vitro folding in nearly native lipid conditions (46). This difference indicates either that current in vitro analysis may be incapable of capturing all the details of SurA-BAM–mediated folding or that additional factors are necessary for proper folding in vivo.

Discussion

Chaperones Are Dynamic uOMP Periplasmic Reservoirs. Because uOMPs are essentially insoluble in monomeric forms in the aqueous milieu of the periplasm (6), periplasmic chaperones are essential for preventing the accumulation of unfolded and aggregated species (12, 26, 27). Our simulations suggest that WT cells maintain a large reservoir of free chaperones while simultaneously creating a situation in which essentially all periplasmic uOMP is bound (Fig. 2 and *SI Appendix*, Fig. S7). These conditions are possible because the apparent total concentration of each chaperone is tuned to be above its respective equilibrium dissociation constant. This thermodynamic finding is complemented by the fact that kinetic rate constants for folding, binding, and unbinding result in chaperone-bound uOMP lifetimes that are orders of magnitude shorter than OMP periplasmic lifetimes. Stated another way: periplasmic chaperones bind their client uOMPs stoichiometrically and are not saturated, and the rates of binding to and dissociating from chaperones are fast (e.g., in milliseconds) relative to folding (*SI Appendix*, Fig. S7) (36). This robust chaperone buffering capacity under WT conditions equips the cell with an ability to cope with mild stress quickly, without the need to wait for a transcriptional regulatory response. More severe stress conditions will cause the population of free uOMP to increase, thus saturating the available chaperone network. Such a condition requires a consequent increase in the concentration of periplasmic chaperones and protease to maintain cell viability—exactly what the σ^E envelope regulatory response is known to accomplish (27). Interestingly, the modulation of only three parameters (chaperone concentration, uOMP synthesis rate, and rate of dilution) within OMPBioM is capable of capturing the expected phenotype of a genetic knockout that induces σ^E.

A Strictly Ordered Set of Reactions Is Not Required to Represent OMP Biogenesis Accurately. There are known examples of escort mechanisms that shuttle molecules across the periplasm via consecutive protein–protein interactions in which the transported molecule is never free in solution (47). Some of these mechanisms involve stable interactions between soluble proteins with binding partners embedded in the inner and outer membranes essentially forming a physical bridge spanning the periplasm. Accordingly, models for OMP biogenesis that have been presented in the literature include a similar, highly ordered mechanism that involves periplasmic chaperones handing uOMP from the Sec translocon to the BAM machinery (48). Evidence for these models includes the in vivo observation of chaperones binding to partially translocated uOMP as well as chaperones interacting with the BAM folding machinery (25, 49). Our model considers neither a sequential set of reactions nor the formation of a multiprotein complex that spans the periplasm. However, OMPBioM still reproduces biological observations. Therefore, these intricate escort mechanisms are not required to explain the process of OMP biogenesis.

Rather, our findings suggest that these biological observations are simply a consequence of the conditions in the periplasm and distinct timescales for key reactions. The abundance of unbound chaperone (*SI Appendix*, Fig. S7) coupled with the fast rates of chaperone binding (e.g., in milliseconds) and the slow rate of translocation (e.g., in seconds) could explain the experimental observation of chaperones binding to uOMP translocation intermediates. Additionally, OMP lifetimes are at least an order of magnitude longer than the timescales necessary for the dissociation of a chaperone–uOMP complex. Therefore, the data to date for OMP maturation can be modeled by simple consideration of thermodynamic and kinetic parameters. This modeling results in a stochastic nondirected process that ends with OMP folding and accurately describes known observables.

One disadvantage of a deterministic treatment is that this methodology cannot track single uOMP trajectories. We therefore complemented our deterministic analysis with stochastic simulations to enumerate the binding events per uOMP. Stochastic simulations result in an average of 348 binding (and unbinding) events per uOMP before folding occurs (Fig. 5*A* and *SI Appendix*, Table S4). Fig. 5*B* shows a representative binding trajectory of a single uOMP, highlighting the stochastic nature of its interactions. Taken together with the prolonged OMP lifetimes (i.e., 59 s) (*SI Appendix*, Table S4), this abundance of chaperone-binding events is not consistent with a continuous physical pathway across the periplasm. Although we recognize that neither computational nor experimental kinetic experiments can disprove a more complex model, the lack of evidence supporting a linear physical pathway for OMP biogenesis and the ability to explain all available data with a

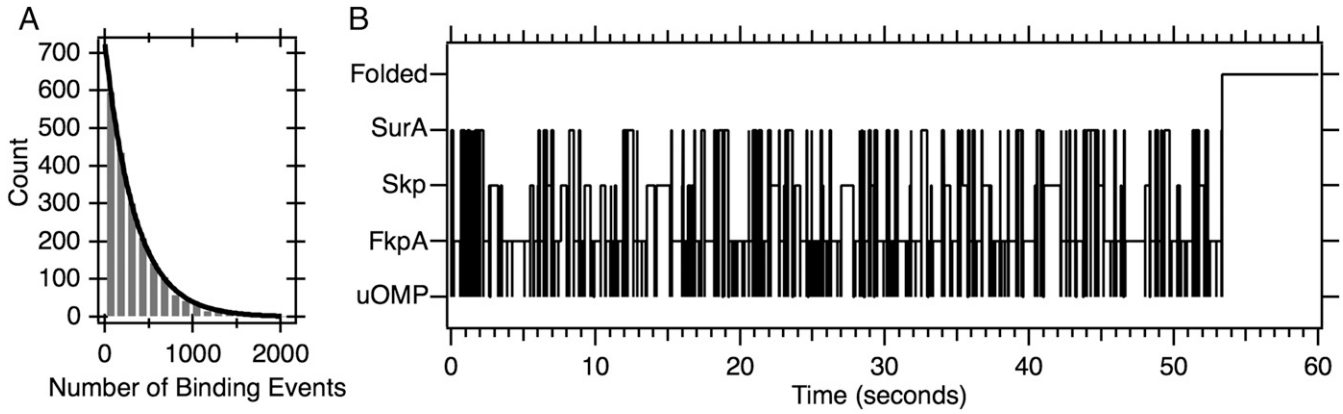

Fig. 5. OMP biogenesis is highly dynamic, with many binding events occurring between uOMP synthesis and folding. (*A*) The number of binding events for each synthesized uOMP under WT conditions. Fitting these data to an exponential decay results in 348 binding events on average. (*B*) A representative trajectory (600,000 steps) of binding events for a single (representative) uOMP over its periplasmic lifetime; between every binding event, the OMP is released to form free uOMP before it is bound by another chaperone. This particular OMP has a periplasmic lifetime of 54 s. *SI Appendix*, Table S4 shows the number of binding events and lifetimes for simulated phenotypes.

simpler mechanism suggest that the treatment presented in this model is the most parsimonious at this time.

Skp and DegP May Not Form a Productive Parallel Folding Pathway. Depletion of either Skp or DegP alone results in a phenotype similar to that of WT, but Δ*surA*Δ*skp* or Δ*surA*Δ*degP* results in a phenotype in which fOMP is depleted from the outer membrane or uOMP is accumulated in the periplasm as compared with the single-null mutant Δ*surA* (Fig. 2) (15, 29). This observation has been used as evidence that Skp and DegP form a folding pathway that is parallel to the SurA–BAM pathway and is essential when SurA is removed from the periplasm (15, 29). Indeed, folding can formally occur in our model from a complex with any chaperone or from free uOMP (Fig. 1). However, we observe negligible folding flux through Skp and DegP because the rate constants used in this mathematical model are relatively low, and neither Skp nor DegP has been shown to interact with the BAM folding machinery.

Nevertheless, to investigate further the role of Skp in catalyzing OMP folding, we increased the folding catalytic activity of Skp to be equal to that of SurA. *SI Appendix*, Fig. S9 shows that the phenotypes resulting from this implementation are not consistent with biological observations. In this hypothetical scenario, none of the Δ*surA* mutants except the double-null Δ*surA*Δ*skp* show perturbations in OMP profiles. Therefore, not only is physiologically relevant folding from Skp or DegP not required; including it in OMPBioM yields phenotypes that are in conflict with experimental results (11–13).

Instead of folding catalytic activity, we suggest the main role of Skp and DegP is quality control under stress conditions. The loss of the folding ability of SurA results in the accumulation of free and aggregated uOMP in the periplasm; under these conditions free uOMP is still able to fold through the BAM pathway but at a slower rate. As a result, the increased levels of uOMP in the periplasm require quality-control mechanisms provided by Skp and DegP to manage this accumulation. Our results suggest that the primary role of these two periplasmic proteins is to assist in quality control under stress conditions and not to form an alternative OMP folding pathway.

Kinetic Partitioning Prevents uOMP Aggregation and Degradation Under WT Conditions. The kinetic and thermodynamic parameters for the intermediate processes in OMP biogenesis are of special interest because of the lack of an external energy source (i.e., ATP) in the periplasm (10). Previous work has suggested that the thermodynamic stability of fOMP drives the partitioning of uOMP from the relatively stable chaperone complexes to the even more stable native state (19). The fact that BamA is essential to cellular viability provides evidence that the kinetics of OMP folding is of the utmost importance as well (40). When known thermodynamic and kinetic parameters are implemented into this model, additional relationships between these two different classes of parameters and this biogenesis pathway are revealed. The relatively slow kinetics of OMP folding result in long periplasmic lifetimes for OMPs, leading to uOMP–chaperone binding reactions poised near equilibrium. Therefore, the populations of free uOMP and chaperone-bound OMP are essentially defined by their binding energies. Under these steady-state conditions, the combination of low free uOMP concentrations and aggregation/degradation rate constants that are even slower than folding rate constants prevents aggregated and degraded OMP species from populating to a significant extent. In essence, such states are kinetically inaccessible despite being thermodynamically favorable. We conclude that a finely tuned balance between thermodynamic and kinetic effects maximizes OMP folding and minimizes aggregation and unnecessary degradation.

Periplasmic Conditions Provide Simple Solutions to Challenges Faced by OMP Biogenesis. OMP biogenesis is subject to obstacles that are not present in cytoplasmic protein-folding systems. OMPBioM simulations indicate that the cell is able to overcome all these barriers simply by regulating the presence of periplasmic chaperones, proteases, and folding catalysts. The folding catalytic ability of BAM and SurA in combination with the chaperone ability of Skp and FkpA and the protease activity of DegP are sufficient to (*i*) prevent an accumulation of free uOMP and therefore aggregated uOMP, (*ii*) overcome the kinetic barriers to folding, (*iii*) maintain fOMP concentrations at sufficient levels, and (*iv*) accomplish all these tasks in the absence of mechanisms that use ATP. The remedy to the many challenges OMPs face during biogenesis is remarkably simple. The inclusion of chaperones and folding catalysts at biologically observed concentrations with binding, aggregation and degradation rates observed in vitro and in vivo results in cellular conditions that promote the efficient folding of OMP and prevent an accumulation of free and aggregated uOMP in the periplasm. Overall, OMPBioM provides a holistic window into understanding how OMP populations are determined by periplasmic processes. This system can be easily modified in the future to incorporate new thermodynamic and kinetic information and for further investigation of any future mechanistic hypotheses for OMP biogenesis.

Methods

Creation of the model is described in *SI Appendix, SI Methods*. *SI Appendix*, Table S1 lists the rate constants used in the model, and *SI Appendix*, Table S2 outlines the set of ordinary differential equations representing all species and reactions in Fig. 1. Deterministic simulations were used to solve the system of equations numerically using Matlab R2014b on a MacBook Pro running OS X Yosemite with a 2.5-GHz Intel Core i5 processor and 8 GB of RAM. The stochastic treatment used a system built in COPASI, where all simulations were performed using the Gibson Bruck method (50).

ACKNOWLEDGMENTS. We thank members of the K.G.F. laboratory for helpful discussions and critical reading of the manuscript and Dr. Elijah Roberts (Johns Hopkins University) for helpful advice. This work was supported by National Science Foundation (NSF) Grant MCB1412108 (to K.G.F.) and NIH Grant R01 GM079440 (to K.G.F.). A.M.P. was supported by NIH Grant T32 GM008403 and is a recipient of NSF Graduate Research Fellowship DGE 1232825. S.M.C. received support from a Provost's Undergraduate Research Award and a Dean's Undergraduate Research Award from Johns Hopkins University and Research Experience for Undergraduates funds through NSF Grant MCB1412108.

1. Tamm LK, Hong H, Liang B (2004) Folding and assembly of β-barrel membrane proteins. *Biochim Biophys Acta - Biomembr* 1666(1-2):250–263.
2. Walther DM, Rapaport D, Tommassen J (2009) Biogenesis of β-barrel membrane proteins in bacteria and eukaryotes: Evolutionary conservation and divergence. *Cell Mol Life Sci* 66(17):2789–2804.
3. Wimley WC (2003) The versatile β-barrel membrane protein. *Curr Opin Struct Biol* 13(4):404–411.
4. Bajaj H, et al. (2012) Antibiotic uptake through membrane channels: Role of Providencia stuartii OmpPst1 porin in carbapenem resistance. *Biochemistry* 51(51):10244–10249.
5. Nikaido H (1989) Outer membrane barrier as a mechanism of antimicrobial resistance. *Antimicrob Agents Chemother* 33(11):1831–1836.
6. Ebie Tan A, Burgess NK, DeAndrade DS, Marold JD, Fleming KG (2010) Self-association of unfolded outer membrane proteins. *Macromol Biosci* 10(7):763–767.
7. Burgess NK, Dao TP, Stanley AM, Fleming KG (2008) β-Barrel proteins that reside in the Escherichia coli outer membrane in vivo demonstrate varied folding behavior in vitro. *J Biol Chem* 283(39):26748–26758.
8. Jarosławski S, Duquesne K, Sturgis JN, Scheuring S (2009) High-resolution architecture of the outer membrane of the Gram-negative bacteria Roseobacter denitrificans. *Mol Microbiol* 74(5):1211–1222.
9. Rassam P, et al. (2015) Supramolecular assemblies underpin turnover of outer membrane proteins in bacteria. *Nature* 523(7560):333–336.
10. Wülfing C, Plückthun A (1994) Protein folding in the periplasm of Escherichia coli. *Mol Microbiol* 12(5):685–692.
11. Ge X, et al. (2014) Identification of FkpA as a key quality control factor for the biogenesis of outer membrane proteins under heat shock conditions. *J Bacteriol* 196(3):672–680.
12. Dartigalongue C, Missiakas D, Raina S (2001) Characterization of the Escherichia coli sigma E regulon. *J Biol Chem* 276(24):20866–20875.
13. Rouvière PE, Gross CA (1996) SurA, a periplasmic protein with peptidyl-prolyl isomerase activity, participates in the assembly of outer membrane porins. *Genes Dev* 10(24):3170–3182.
14. Bitto E, McKay DB (2004) Binding of phage-display-selected peptides to the periplasmic chaperone protein SurA mimics binding of unfolded outer membrane proteins. *FEBS Lett* 568(1-3):94–98.
15. Sklar JG, Wu T, Kahne D, Silhavy TJ (2007) Defining the roles of the periplasmic chaperones SurA, Skp, and DegP in Escherichia coli. *Genes Dev* 21(19):2473–2484.
16. Lazar SW, Kolter R (1996) SurA assists the folding of Escherichia coli outer membrane proteins. *J Bacteriol* 178(6):1770–1773.
17. Vuong P, Bennion D, Mantei J, Frost D, Misra R (2008) Analysis of YfgL and YaeT interactions through bioinformatics, mutagenesis, and biochemistry. *J Bacteriol* 190(5):1507–1517.
18. Gessmann D, et al. (2014) Outer membrane β-barrel protein folding is physically controlled by periplasmic lipid head groups and BamA. *Proc Natl Acad Sci USA* 111(16):5878–5883.
19. Moon CP, Zaccai NR, Fleming PJ, Gessmann D, Fleming KG (2013) Membrane protein thermodynamic stability may serve as the energy sink for sorting in the periplasm. *Proc Natl Acad Sci USA* 110(11):4285–4290.
20. Plummer AM, Fleming KG (2015) BamA Alone Accelerates Outer Membrane Protein Folding In Vitro through a Catalytic Mechanism. *Biochemistry* 54(39):6009–6011.
21. Wu T, et al. (2005) Identification of a multicomponent complex required for outer membrane biogenesis in Escherichia coli. *Cell* 121(2):235–245.
22. Thoma J, Burmann BM, Hiller S, Müller DJ (2015) Impact of holdase chaperones Skp and SurA on the folding of β-barrel outer-membrane proteins. *Nat Struct Mol Biol* 22(10):795–802.
23. Masuda T, Saito N, Tomita M, Ishihama Y (2009) Unbiased quantitation of Escherichia coli membrane proteome using phase transfer surfactants. *Mol Cell Proteomics* 8(12):2770–2777.
24. Ishihama Y, et al. (2008) Protein abundance profiling of the Escherichia coli cytosol. *BMC Genomics* 9:102.
25. Ureta AR, Endres RG, Wingreen NS, Silhavy TJ (2007) Kinetic analysis of the assembly of the outer membrane protein LamB in Escherichia coli mutants each lacking a secretion or targeting factor in a different cellular compartment. *J Bacteriol* 189(2):446–454.
26. Onufryk C, Crouch M-L, Fang FC, Gross CA (2005) Characterization of six lipoproteins in the sigmaE regulon. *J Bacteriol* 187(13):4552–4561.
27. Rhodius VA, Suh WC, Nonaka G, West J, Gross CA (2006) Conserved and variable functions of the σE stress response in related genomes. *PLoS Biol* 4(1):0043–0059.
28. Mecsas J, Rouviere PE, Erickson JW, Donohue TJ, Gross CA (1993) The activity of sigma E, an Escherichia coli heat-inducible sigma-factor, is modulated by expression of outer membrane proteins. *Genes Dev* 7(12B):2618–2628.
29. Rizzitello AE, Harper JR, Silhavy TJ (2001) Genetic evidence for parallel pathways of chaperone activity in the periplasm of Escherichia coli. *J Bacteriol* 183(23):6794–6800.
30. Ge X, et al. (2014) DegP primarily functions as a protease for the biogenesis of β-barrel outer membrane proteins in the Gram-negative bacterium Escherichia coli. *FEBS J* 281(4):1226–1240.
31. Strauch KL, Johnson K, Beckwith J (1989) Characterization of degP, a gene required for proteolysis in the cell envelope and essential for growth of Escherichia coli at high temperature. *J Bacteriol* 171(5):2689–2696.
32. Krojer T, et al. (2008) Structural basis for the regulated protease and chaperone function of DegP. *Nature* 453(7197):885–890.
33. CastilloKeller M, Misra R (2003) Protease-deficient DegP suppresses lethal effects of a mutant OmpC protein by its capture. *J Bacteriol* 185(1):148–154.
34. Walton TA, Sousa MC (2004) Crystal structure of Skp, a prefoldin-like chaperone that protects soluble and membrane proteins from aggregation. *Mol Cell* 15(3):367–374.
35. McMorran LM, Bartlett AI, Huysmans GHM, Radford SE, Brockwell DJ (2013) Dissecting the effects of periplasmic chaperones on the in vitro folding of the outer membrane protein PagP. *J Mol Biol* 425(17):3178–3191.
36. Wu S, et al. (2011) Interaction between bacterial outer membrane proteins and periplasmic quality control factors: A kinetic partitioning mechanism. *Biochem J* 438(3):505–511.
37. Lazar SW, Almirón M, Tormo A, Kolter R (1998) Role of the Escherichia coli SurA protein in stationary-phase survival. *J Bacteriol* 180(21):5704–5711.
38. Rothman JE (1989) Polypeptide chain binding proteins: Catalysts of protein folding and related processes in cells. *Cell* 59(4):591–601.
39. Fleming KG (2015) A combined kinetic push and thermodynamic pull as driving forces for outer membrane protein sorting and folding in bacteria. *Philos Trans R Soc B* 370:20150026.
40. Voulhoux R, Bos MP, Geurtsen J, Mols M, Tommassen J (2003) Role of a highly conserved bacterial protein in outer membrane protein assembly. *Science* 299(5604):262–265.
41. Noinaj N, et al. (2013) Structural insight into the biogenesis of β-barrel membrane proteins. *Nature* 501(7467):385–390.
42. Noinaj N, Kuszak AJ, Balusek C, Gumbart JC, Buchanan SK (2014) Lateral opening and exit pore formation are required for BamA function. *Structure* 22(7):1055–1062.
43. Danoff EJ, Fleming KG (2015) Membrane defects accelerate outer membrane β-barrel protein folding. *Biochemistry* 54(2):97–99.
44. Bakelar J, Buchanan SK, Noinaj N (2016) The structure of the β-barrel assembly machinery complex. *Science* 351(6269):180–186.
45. Malinverni JC, et al. (2006) YfiO stabilizes the YaeT complex and is essential for outer membrane protein assembly in Escherichia coli. *Mol Microbiol* 61(1):151–164.
46. Hagan CL, Kahne D (2011) The reconstituted Escherichia coli Bam complex catalyzes multiple rounds of β-barrel assembly. *Biochemistry* 50(35):7444–7446.
47. May JM, Sherman DJ, Simpson BW, Ruiz N, Kahne D (2015) Lipopolysaccharide transport to the cell surface: Periplasmic transport and assembly into the outer membrane. *Philos Trans R Soc B* 370:20150027.
48. Lyu ZX, Zhao XS (2015) Periplasmic quality control in biogenesis of outer membrane proteins. *Biochem Soc Trans* 43(2):133–138.
49. Harms N, et al. (2001) The early interaction of the outer membrane protein phoe with the periplasmic chaperone Skp occurs at the cytoplasmic membrane. *J Biol Chem* 276(22):18804–18811.
50. Gibson MA, Bruck J (2000) Efficient exact stochastic simulation of chemical systems with many species and many channels. *J Phys Chem* 104(9):1876–1889.